

IGNIT3: AN INTEGRATED COMPUTATIONAL FRAMEWORK FOR NON-IDEAL THERMODYNAMIC ANALYSIS AND OPTIMIZATION OF TURBOJET AND TURBOFAN ENGINES

Pablo Gonzales-DeGreiff[1], Juan Gonzalez-Mitte[2], Giuseppe Palaia[3], Karim Abu Salem[3] & Pedro D Bravo-Mosquera[2]

[1]New Granada Military University (UMNG), Cajicá, Cundinamarca, Colombia
[2]São Carlos School of Engineering, University of São Paulo (EESC / USP), São Carlos, SP, Brazil
[3]Department of Mechanical and Aerospace Engineering, Politecnico di Torino, 10129 Turin, Italy

Abstract

IGNIT3 (Integrated Gas Non-Ideal Thermodynamic Turbofan and Turbojet Evaluation) is a modular computational framework developed for the thermodynamic analysis and optimization of turbojet and turbofan engines. The code is based on fundamental principles of thermodynamics and fluid mechanics, with explicit consideration of non-ideal gas effects throughout the propulsion cycle. The methodology relies on an interconnected system of calculation modules representing the main engine components, enabling the complete analysis of the thermodynamic cycle from inlet to nozzle. By prescribing initial conditions, such as ambient conditions, component efficiencies, and design parameters, the framework computes key performance metrics including thrust, thermal and propulsive efficiency, specific fuel consumption (SFC), temperature and pressure distributions at critical engine stations. The formulation accommodates different engine configurations, including fixed or variable geometry nozzles, the presence or absence of an afterburner, and alternative assumptions for mixer chamber pressure. The results demonstrate the capability of IGNIT3 to support preliminary design studies and optimization-oriented investigations, offering a flexible and robust tool for research, education, and early-stage propulsion system development.

Keywords: Thermodynamic cycle; Turbofan; Turbojet; Off-design performance; Specific Fuel Consumption

1. Introduction

The development of aircraft engines represents a core discipline within aerospace engineering, exerting a decisive influence on aircraft performance, operational efficiency, and mission requirements. Propulsion systems are required to operate safely and reliably under severe thermal, mechanical, and aerodynamic loading conditions while maintaining strict tolerances over extended service lives [1]. These constraints impose demands on the robustness of thermodynamic cycle design and on the accuracy of performance prediction methodologies applied during the preliminary phases of engine development.

From a systems-level perspective, engine design governs thrust generation and fuel consumption, with aircraft-level performance benefits emerging primarily through reductions in specific fuel consumption (SFC). Improvements in SFC translate directly into reduced mission fuel requirements, enabling greater flexibility in aircraft operation under fixed weight and mission constraints. Therefore, accurate prediction of SFC across operating conditions is central to assess the system-level impact of propulsion design choices. In parallel, modern aircraft engine design is increasingly driven by the need for improved efficiency, reduced environmental impact, and continued technological advancement. The transition from turbojet to turbofan architectures has demonstrated the benefits of accelerating larger air masses at lower jet velocities, leading to significant reductions in fuel consumption and

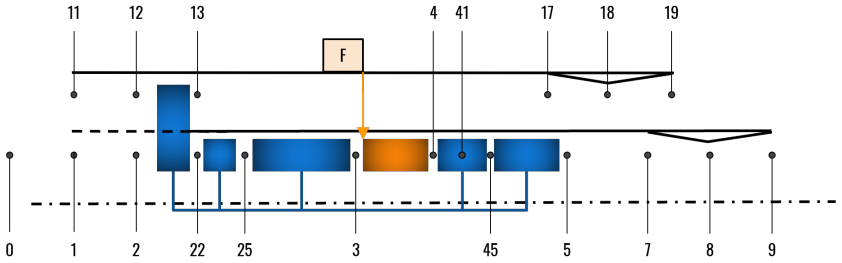
operating costs [2]. At the same time, new regulations on emissions and noise have motivated the development of advanced propulsion concepts, including adaptive cycle engines and hybrid-electric systems aimed at long-term sustainability objectives. Continuous innovations in engine technology, such as advances in compressor design, high-temperature materials, and variable-geometry components, have enabled improvements not only in propulsion efficiency but also in aircraft aerodynamic integration and overall system performance.

During the preliminary phases of aircraft engine design, cycle analysis tools are essential to explore design spaces, evaluate trade-offs, and guide configuration choices prior to detailed component-level development. Classical gas turbine analysis methods, widely adopted in propulsion textbooks and preliminary design frameworks, rely on simplified thermodynamic assumptions to enable analytical tractability and rapid performance evaluation, most notably the treatment of the working fluid as a calorically perfect gas with constant heat capacity ratio (γ). While these assumptions provide valuable physical insight into the fundamental behavior of turbojet and turbofan engines, their limitations become increasingly apparent for engines operating at high turbine inlet temperatures, across wide flight envelopes, or under off-design conditions [3]. In such regimes, the temperature dependence of thermodynamic properties and non-ideal gas effects can significantly influence predicted thrust, efficiency, and fuel consumption, reducing the accuracy of conventional cycle-based performance estimates.

Several studies have addressed these limitations by introducing progressively more realistic thermodynamic modeling. Grönstedt [4] presented the development of GESTPAN, a computational framework intended for the conceptual design and performance simulation of gas turbine engines under both steady and transient operating conditions. The methodology integrates engine cycle definition with the optimization of variable-geometry control strategies to improve system analysis and operational flexibility. Liew et al [5] developed a parametric cycle analysis of a turbofan engine with an interstage turbine burner. The authors demonstrated that variable specific heats affect predicted thrust, fuel consumption, and component matching, particularly at elevated turbine inlet temperatures. These results highlighted that constant assumptions of γ can introduce systematic errors in cycle efficiency and specific thrust predictions, motivating the development of variable-property cycle solvers. NASA technical reports have played a central role in advancing thermodynamic modeling fidelity for propulsion systems. Jones [6] introduced the analysis of gas turbine engine cycles using the Numerical Propulsion System Simulation (NPSS) code. This framework integrates disciplines such as aerodynamics and heat transfer to simulate steady-state or transient engine cycles, enabling detailed analysis by linking different fidelity component models and supporting collaborative engineering for complex propulsion system development [7, 8]. More research has explored intermediate-fidelity approaches that balance physical realism and computational efficiency. Rangwala and Wilson [9] investigated variable specific heat formulations within cycle-based solvers, demonstrating that incorporating temperature-dependent specific heat at constant pressure (C_p) and heat capacity ratio (γ) is particularly important for engines with afterburners, high overall pressure ratios, and strong mixing effects, where thermodynamic nonlinearity is pronounced.

More recently, Hendricks and Gray [10] introduced a framework for efficient optimization of gas turbine engine cycles (pyCycle). This tool is structured around a modular and extensible architecture designed to support the thermodynamic evaluation of a wide range of engine configurations and operating conditions. The framework employs a cycle-based formulation that enables systematic analysis of complete propulsion systems while accounting for non-ideal thermodynamic behavior. Numerical iteration schemes are used to ensure consistent coupling between engine components, particularly in the treatment of flow equilibrium in elements such as mixers and nozzles, thereby enhancing robustness when analyzing complex configurations, including mixed-flow turbofan architectures [11].

Based on the gaps and challenges identified in the literature, IGNIT3 integrates variable thermodynamic properties directly into engine cycle analysis. This formulation enables the framework to cap-



Station	Description
0	Free-stream
11	Diffuser - external fan
1	Diffuser - internal fan
12	Inlet - external fan
2	Inlet - internal fan
13	Fan nozzle - external fan
22	Fan nozzle - internal fan / Inlet LPC
25	Outlet - LPC / Inlet HPC
3	Outlet - HPC / Inlet combustor

4	Outlet combustor / Inlet stator NGV HPT
41	HPT NGV outlet / HPT rotor inlet
45	LPT inlet
5	LPT outlet
17	Inlet - Bypass duct nozzle
18	Throat - Bypass duct nozzle
19	Outlet - Bypass duct nozzle
7	Inlet - Core duct nozzle
8	Throat - Core duct nozzle
9	Outlet - Core duct nozzle

Figure 1 – Standardized station numbering adopted in the IGNIT3 framework.

ture the influence of thermal-property variations on compression, combustion, expansion, and mixing processes without the computational overhead associated with full equilibrium chemistry solvers. By combining thermodynamic property variation with iterative numerical methods, such as the regula falsi technique for mixer pressure equilibrium, IGNIT3 bridges the methodological gap between simplified analytical cycle models and high-fidelity propulsion simulation environments. The framework aligns with contemporary directions in propulsion research that emphasize physical consistency, modularity, and computational accessibility for parametric studies, design optimization, and educational applications.

2. Methodology

The IGNIT3 framework adopts a modular, cycle-based methodology for the thermodynamic analysis of turbojet and turbofan engines, with explicit consideration of temperature-dependent gas properties and component-level coupling. The methodology is structured to support both design-point and off-design analyses while maintaining a balance between physical fidelity and computational efficiency.

2.1 Software Architecture

Figure 1 illustrates the standardized station numbering adopted in the IGNIT3 framework for the thermodynamic analysis of a turbofan engine. The schematic represents the axial layout of the engine, highlighting the main flow path through the inlet, fan, compressors, combustor, turbines, and exhaust systems, as well as the bypass stream. Each component interface is associated with a specific station number, enabling a consistent definition of thermodynamic states throughout the propulsion system. The engine architecture is controlled by Boolean activation flags listed in Table 1. This modular strategy enables the simulation of multiple engine architectures, from basic turbojet arrangements to advanced three-spool mixed-flow turbofan configurations with afterburning, using a unified set of component models.

2.1.1 Temperature-Dependent Thermodynamic Properties

Unlike simplified models that assume constant thermodynamic properties, the present implementation dynamically evaluates the specific heat ratio γ as a function of temperature. This is an empirical model describing how the specific heat (c_p) of a gas varies with the temperature (T) in Kelvin. The exponential form is very common when specific heat increases smoothly with temperature [12].

Table 1 – IGNIT3 stage activation flags and their effect on engine architecture.

Flag	Component	Effect
`fan_act`	Fan and bypass duct	Enables turbofan mode
`compLP_act`	LP compressor	Activates first compression spool
`spoolIP_act`	IP compressor/turbine	Adds intermediate spool (Spool 2)
`spoolHP_act`	HP compressor/turbine	Adds high-pressure spool (Spool 3)
`mix_act`	Mixer and bypass duct	Enables mixed-flow turbofan cycle
`after_act`	Afterburner	Adds reheat combustion stage
`nozzle_var`	Primary nozzle	Selects variable vs. fixed geometry
`fnozzle_var`	Fan nozzle type	Selects variable vs. fixed geometry

$$c_p = 0.95032 e^{0.000175T} \tag{1}$$

The ratio of specific heats is subsequently obtained through:

$$\gamma = \frac{c_p}{c_p - R} \tag{2}$$

where $R = 0.28704$ kJ kg^{-1}K^{-1} is the specific gas constant for air. Both c_p and γ are evaluated at the arithmetic mean of the component inlet and exit stagnation temperatures, and are solved simultaneously with the exit temperature through a coupled nonlinear system. Specific entropy differences are computed consistently using the ideal-gas Gibbs relation:

$$s_2 - s_1 = c_p \ln\frac{T_{02}}{T_{01}} - R \ln\frac{P_{02}}{P_{01}} \tag{3}$$

This entropy formulation is used by each component both to advance the thermodynamic state and to generate the temperature–entropy (T–s) diagram.

2.1.2 Design-Point

The design-point analysis is performed automatically during the initialization of the main module. This procedure establishes the baseline engine configuration that corresponds to a prescribed operating condition. The thermodynamic cycle is solved sequentially through all engine components, beginning with the diffuser and ending at the exhaust nozzles.

For mixed-flow turbofan configurations, the framework incorporates an iterative mixer balancing procedure during the design-point calculation. In mixed-flow engines, the bypass stream and the hot core stream must reach compatible pressure conditions before entering the mixer chamber. If the pressures differ excessively, the mixing process becomes physically inconsistent and may lead to inaccurate thrust predictions. To resolve this issue, the framework iteratively adjusts the fan pressure ratio using the Regula Falsi method until pressure equilibrium is achieved between the two streams.

The convergence criterion is defined as: $|P_{core} - P_{bypass}| < 10^{-5}$. The iterative correction of the fan pressure ratio is one of the most advanced features of the framework, since it effectively performs an internal aerodynamic matching process between the core and bypass streams. Three distinct mass flow streams are tracked throughout the on-design cycle: the core stream ($\dot{m}_1$), the fan bypass stream ($\dot{m}_2$), and a duct split stream ($\dot{m}_3$) extracted from the bypass flow prior to the mixer. The total ingested mass flow ($\dot{m}_0$) is divided at the fan exit according to the bypass ratio ($\mathscr{B}$) and the duct split ratio (σ):

$$\dot{m}_0 = \dot{m}_1 + \dot{m}_2, \qquad \mathscr{B} = \frac{\dot{m}_2}{\dot{m}_1}, \qquad \dot{m}_3 = \sigma \dot{m}_2 \tag{4}$$

The fuel mass flow rate ($\dot{m}_f$) introduced in the combustor and afterburner is included in the nozzle mass balance to ensure accurate evaluation of the exhaust mass flow rate and net thrust.

2.1.3 Off-Design Analysis

The off-design analysis is integrated to a single design point defined by the flight condition, the core mass flow rate, and the component pressure ratios and efficiencies. All off-design quantities are expressed as deviations from this reference. The corrected flow function gives the actual mass flow per unit area at a cross-section in terms of the stagnation conditions:

$$\frac{\dot{m}}{A} = \frac{P_0\sqrt{\gamma}}{\sqrt{RT_0}} M \left(\frac{1}{1+\frac{\gamma-1}{2}M^2} \right)^{\frac{\gamma+1}{2(\gamma-1)}} \tag{5}$$

where M is the flight Mach number and T_0 and P_0 are the stagnation temperature and pressure, respectively.

Instead of using an analytical map formulation, the present work employs a map scaling approach similar to that implemented in NNEP program [13]. These maps, derived from representative axial-flow turbomachinery, provide physically consistent performance trends and can be scaled within reasonable limits to represent similar engine architectures. All map quantities are expressed in terms of corrected variables, which collapse the effects of varying inlet temperature and pressure onto a single characteristic surface. The temperature and pressure correction factors at the inlet of each component are:

$$\theta = \frac{T_{01}}{T_{\text{ref}}} = \frac{T_{01}}{288.15\,\text{K}} \qquad \delta = \frac{P_{01}}{P_{\text{ref}}} = \frac{P_{01}}{101.325\,\text{kPa}} \tag{6}$$

where T_{01} and P_{01} are the stagnation temperature and pressure at the component inlet, and the reference conditions correspond to ISA sea-level standard values. The corrected mass flow rate, which is analogous to Eq. 5 is:

$$W_C = \dot{m}\frac{\sqrt{\theta}}{\delta} \propto \frac{AM_{max}\sqrt{\gamma/R}}{\left(1+\frac{\gamma-1}{2}M_{max}^2\right)^{\frac{\gamma+1}{2(\gamma-1)}}} \tag{7}$$

where W_C represents the axial Mach number in an annular area compressor A. M_{max} for compressors is usually lower than 0.7 and is physically limited to 1.0 for choke conditions. The corrected shaft speed is expressed as a normalized ratio:

$$\bar{N} = \frac{N}{\sqrt{\theta}} \propto \frac{U}{\sqrt{T}} = M_U \frac{\sqrt{\gamma/R}}{\sqrt{1+\frac{\gamma-1}{2}M_{max}^2}} \tag{8}$$

where $\bar{N} = 1$ at the design point and M_U represents the tangential Mach number, which can take any value, including values greater than 1.0, but is usually limited by M_{max}. Any combination of altitude and Mach number that yields the same corrected mass flow and corrected rotational speed corresponds to the same non-dimensional operating point. Under similarity assumptions, this results in the same pressure ratio, temperature ratio, and isentropic efficiency. The reference map represents the performance characteristics of a generic turbomachine. To adapt it to a specific engine, the map coordinates are scaled such that the reference map design point coincides with the design operating point predicted by IGNIT3 $(W_{C,D}, \pi_D)$.

A fundamental difficulty in compressor map representation arises near the surge boundary, where speed lines become nearly vertical in the (W_C, π) plane. In this region, W_C is no longer a unique coordinate for locating an operating point on a given speed line, since a single W_C value may correspond to two different values of pressure ratio (π) on the same speed line. The Beta line parametrization resolves this ambiguity by introducing an auxiliary coordinate $\beta \in [0,1]$ that runs monotonically from the choke end ($\beta = 0$) to the surge end ($\beta = 1.0$) along each speed line [14].

For each scaled speed line i containing n_i tabulated points, the N_β beta anchor positions are sampled at uniformly spaced indices:

$$k_j = \text{round}\left(1 + \frac{j-1}{N_\beta - 1}\,(n_i - 1)\right) \qquad j = 1, 2, \ldots, N_\beta \tag{9}$$

The corresponding anchor coordinates are:

$$\left(W_C^{(i,j)},\ \pi^{(i,j)}\right) = \left(W_C^{scaled}[k_j],\ \pi^{scaled}[k_j]\right) \tag{10}$$

This yields an anchor table of dimensions $N_{speeds} \times N_\beta$, where N_{speeds} is the number of speed lines in the map. The surge and choke lines are derived directly from the endpoints of the tabulated lines. The surge margin is defined as:

$$SM(W_C) = \frac{\pi_{surge}(W_C)}{\pi(W_C)} - 1 \tag{11}$$

where $\pi(W_C)$ is the compressor pressure ratio at the current operating point and $\pi_{surge}(W_C)$ is the pressure ratio corresponding to the surge line at the same corrected mass flow rate. This definition expresses the relative distance between the operating point and the surge boundary in terms of pressure ratio. A positive surge margin indicates stable operation, whereas a surge margin approaching zero signifies that the compressor is operating near the onset of surge.

2.1.4 Thrust and Specific Fuel Consumption

Net thrust is computed by summing the momentum and pressure thrust contributions of both nozzle streams:

$$F_{\text{net}} = \underbrace{\dot{m}_9 V_9 - \dot{m}_0 V_0 + (P_9 - P_a) A_9}_{\text{core nozzle}} + \underbrace{\dot{m}_{19} V_{19} - \dot{m}_0 V_0 + (P_{19} - P_a) A_{19}}_{\text{fan nozzle}} \tag{12}$$

where subscripts 9 and 19 denote the core and fan nozzle exit planes, respectively, $\dot{m}_0 V_0$ is the ram drag component, V is the exhaust velocity, P is the static exit pressure, P_a is the freestream static pressure, and A is the nozzle exit area. The thrust-specific fuel consumption (TSFC) is then obtained by:

$$\text{TSFC} = \frac{\dot{m}_{f,\text{tot}}}{F_{\text{net}}} \cdot 3600 \quad [\text{kg h}^{-1}\,\text{N}^{-1}] \tag{13}$$

where $\dot{m}_{f,\text{tot}}$ is the total fuel mass flow rate summed across the combustor and afterburner.

2.1.5 Cycle Efficiencies

The IGNIT3 on-design evaluates three efficiency metrics that characterize the energy conversion chain of the engine: *thermal efficiency*, which measures how effectively the chemical energy of the fuel is converted into net kinetic energy of the flow; *propulsive efficiency*, which measures how effectively that net kinetic energy is converted into useful propulsive work; and *overall efficiency*, the product of the two.

The kinetic energy flux leaving the engine is the sum of the contributions from the primary nozzle and the fan nozzle:

$$\dot{KE}_{out} = \tfrac{1}{2}\,\dot{m}_p\,u_{j,p}^2 + \tfrac{1}{2}\,\dot{m}_f\,u_{j,f}^2 \tag{14}$$

where $\dot{m}_p$ and $u_{j,p}$ are the mass flow and jet velocity of the primary nozzle, and $\dot{m}_f$ and $u_{j,f}$ are the corresponding quantities for the fan nozzle. For a pure turbojet the fan-nozzle term vanishes. The kinetic energy flux entering the engine with the freestream is:

$$\dot{KE}_{in} = \tfrac{1}{2}\,\dot{m}_{in}\,V_\infty^2 \tag{15}$$

where $\dot{m}_{in}$ is the total ingested mass flow at the diffuser and V_∞ is the freestream (flight) velocity. The net rate of kinetic energy added to the flow by the engine is:

$$\dot{KE}_{net} = \dot{KE}_{out} - \dot{KE}_{in} \tag{16}$$

The rate of chemical energy supplied by the fuel is:

$$\dot{E}_{fuel} = \dot{m}_{fuel} \cdot LHV \tag{17}$$

where $\dot{m}_{fuel}$ is the total fuel mass flow (including any afterburner contribution) and LHV is the lower heating value of the fuel. The thermal efficiency is defined as the ratio of the net kinetic energy added to the flow to the chemical energy released by the fuel:

$$\eta_{th} = \frac{\dot{KE}_{net}}{\dot{E}_{fuel}} = \frac{\frac{1}{2}\dot{m}_p u_{j,p}^2 + \frac{1}{2}\dot{m}_f u_{j,f}^2 - \frac{1}{2}\dot{m}_{in} V_\infty^2}{\dot{m}_{fuel} \cdot LHV} \tag{18}$$

This metric quantifies the effectiveness of the thermodynamic cycle in converting fuel energy into a net increase of flow kinetic energy. The propulsive efficiency is defined as the ratio of the useful propulsive power (the product of net thrust and flight velocity) to the net kinetic energy added to the flow:

$$\eta_{prop} = \frac{F_{net} V_\infty}{\dot{KE}_{net}} \tag{19}$$

where F_{net} is the net thrust of the engine, computed as the sum of the momentum and pressure thrust contributions of both nozzles:

$$F_{net} = F_{mom,p} + F_{pres,p} + F_{mom,f} + F_{pres,f} \tag{20}$$

The propulsive efficiency measures how effectively the kinetic energy imparted to the flow is converted into useful thrust work. When $\dot{KE}_{net} \leq 0$, the propulsive efficiency is set to zero in the implementation to avoid a non-physical result. The overall efficiency is the product of the thermal and propulsive efficiencies:

$$\eta_{ov} = \eta_{th} \cdot \eta_{prop} \tag{21}$$

Substituting the definitions of Eqs. (18) and (19), the net kinetic energy term cancels, yielding the equivalent direct form:

$$\eta_{ov} = \frac{F_{net} V_\infty}{\dot{E}_{fuel}} = \frac{F_{net} V_\infty}{\dot{m}_{fuel} \cdot LHV} \tag{22}$$

which expresses the useful propulsive power as a fraction of the total chemical energy supplied — the fundamental measure of engine fuel-economy performance.

2.2 Component models

The implementation follows an Object-Oriented architecture, providing a modular framework based on reusable components. Thus, each object represents a specific engine module, containing its own thermodynamic processes, governing equations, input parameters, and output variables.

2.2.1 Diffuser

The diffuser class represents the inlet compression system of the propulsion framework and is responsible for modeling the thermodynamic transformation between freestream atmospheric conditions and the compressor inlet conditions. The diffuser model computes the conversion of incoming kinetic energy into stagnation pressure while accounting for compressibility effects, atmospheric conditions, and pressure losses. The implementation supports both subsonic and supersonic inlet conditions, enabling the simulation of a broad range of flight regimes.

The model receives the flight Mach number, geopotential altitude, and ingested air mass flow rate as input parameters, and evaluates the corresponding stagnation properties, entropy variation, and

total pressure recovery throughout the intake system. The stagnation temperature at the diffuser lip is computed from the isentropic energy equation:

$$\frac{T_0}{T_a} = 1 + \frac{\gamma - 1}{2} M^2 \tag{23}$$

The stagnation pressure at the diffuser lip is evaluated through the isentropic relation:

$$\frac{P_0}{P_a} = \left(\frac{T_0}{T_a} \right)^{\gamma/(\gamma-1)} \tag{24}$$

and the diffuser exit pressure is corrected using a prescribed pressure recovery factor:

$$P_2 = \eta_d \cdot P_0 \tag{25}$$

where η_d represents the diffuser pressure recovery. For supersonic operating conditions ($M \geq 1$), the diffuser incorporates normal shock relations to model the deceleration process before the compressor face. The downstream Mach number is obtained from:

$$M_2^2 = \frac{(\gamma - 1) M^2 + 2}{2\gamma M^2 - (\gamma - 1)} \tag{26}$$

2.3 Compressor

The compressor module computes the thermodynamic state of the working fluid after a compression process based on the specified pressure ratio and isentropic efficiency. The inlet stagnation temperature, stagnation pressure, mass flow rate, and entropy are inherited from the upstream engine component.

The engine may have up to three spools, each with a corresponding compressor object. The compressors receive the incoming air from the inlet or the previous spool's compressor and sequentially compress it. Each compressor applies compression processes to increase the air pressure and temperature. The compressed air from each spool is then passed to the combustor or mixed with bypass air.

Given the inlet stagnation temperature T_{02}, the imposed pressure ratio π_c, and the isentropic efficiency η_c, the exit stagnation temperature is determined by solving the following system for γ and T_{03}:

$$\begin{cases} \gamma = \dfrac{c_p\left(\frac{T_{02}+T_{03}}{2}\right)}{c_p\left(\frac{T_{02}+T_{03}}{2}\right) - R} \\ \dfrac{T_{03}}{T_{02}} = 1 + \dfrac{\pi_c^{(\gamma-1)/\gamma} - 1}{\eta_c} \end{cases} \tag{27}$$

The exit stagnation pressure is:

$$P_{03} = \pi_c P_{02} \tag{28}$$

The shaft power absorbed by the compressor stage is:

$$\dot{W}_c = \dot{m}_{out}\, c_p\, (T_{03} - T_{02}) = \frac{\dot{m}_{out}\, c_p T_{02} \left(\gamma^{\frac{\gamma-1}{\gamma}} - 1 \right)}{\eta_c} \tag{29}$$

where $\dot{m}_{out}$ is the compressor exit mass flow. For the fan, $\dot{m}_{out}$ includes both the core and bypass streams, with the split applied downstream by the mixer module.

2.4 Combustor

The combustor module receives the compressed air from the final spool's compressor and mixes it with fuel. It models the combustion process, accounting for heat release and the resulting increase in temperature and pressure. The combustor produces high-pressure, high-temperature gases that are directed to the turbines.

The combustor is modeled as a constant-pressure heat addition process with a prescribed exit stagnation temperature T_{04} (turbine inlet temperature, TIT) and a combustor pressure ratio $\pi_b < 1$ that accounts for friction and heat transfer losses.

The fuel mass flow required to achieve the specified TIT is derived from the steady-flow energy equation with combustion efficiency η_b:

$$\dot{m}_f = \frac{-c_p \dot{m}_{03} (T_{03} - T_{04})}{\eta_b LHV - c_p T_{04}} \tag{30}$$

where LHV is the lower heating value of the fuel (kJ/kg) and $\dot{m}_{03}$ is the inlet air mass flow, and η_b is the burner efficiency. The exit mass flow is:

$$\dot{m}_{04} = \dot{m}_{03} + \dot{m}_f \tag{31}$$

The same class is reused for the afterburner with an independently specified exit temperature and efficiency.

2.5 Turbine

Each turbine stage extracts exactly the shaft power demanded by its mechanically coupled compressor stage, accounting for the shaft mechanical efficiency η_m. The exit stagnation temperature T_{05} is found by solving:

$$\begin{cases} \gamma = \dfrac{c_p\left(\frac{T_{04}+T_{05}}{2}\right)}{c_p\left(\frac{T_{04}+T_{05}}{2}\right) - R} \\ \dot{W}_{req} = \eta_m \dot{m}_{04} c_p\left(\frac{T_{04}+T_{05}}{2}\right)(T_{04} - T_{05}) \end{cases} \tag{32}$$

where $\dot{W}_{req}$ is the total shaft power requirement of the coupled compressor and fan stages. The turbine temperature ratio is:

$$\tau_t = \frac{T_{05}}{T_{04}} \tag{33}$$

The turbine pressure ratio is obtained from the isentropic relation corrected for the turbine isentropic efficiency η_t:

$$\pi_t = \left(1 - \frac{1 - \tau_t}{\eta_t}\right)^{\gamma/(\gamma-1)} \tag{34}$$

$$P_{05} = \pi_t P_{04} \tag{35}$$

In a multi-spool architecture, the high-pressure turbine powers the HP compressor, the intermediate-pressure turbine powers the IP compressor, and the low-pressure turbine powers both the LP compressor and the fan. Each spool is solved independently in that order.

2.6 Bypass Duct and Mixer Chamber

When the mixer is active, a fraction of the fan exit flow is directed through the bypass duct before being combined with the core stream from the LP turbine exit in the mixer chamber.

The bypass duct applies a pressure loss characterized by the pressure ratio of the duct π_{duct}:

$$P_{0,16} = \pi_{duct}\, P_{0,13} \tag{36}$$

The stagnation temperature is assumed to remain constant across the duct ($T_{0,16} = T_{0,13}$), consistent with an adiabatic duct. A fraction SR (split ratio) of the bypass mass flow is admitted to the mixer, while the remainder $(1 - SR)$ is directed to the fan nozzle:

$$\dot{m}_{mix,duct} = SR \cdot \dot{m}_{bypass} \qquad \dot{m}_{fannozzle} = (1 - SR) \cdot \dot{m}_{bypass} \tag{37}$$

For the mixing process to be physically consistent, the static pressures of the two streams at the mixer inlet must be equal. Since the fan pressure ratio is not known a priori, IGNIT3 uses the Regula Falsi method to iteratively adjust the fan pressure ratio until the pressure difference at the mixer inlet satisfies:

$$\Delta P_{mix} = P_{0,duct} - P_{0,core} \to 0 \tag{38}$$

Convergence is declared when $|\Delta P_{mix}| < 10^{-5}$ kPa or after 50 iterations. The mixer exit stagnation temperature T_{06} is obtained from the steady-flow energy balance, solved implicitly because c_p depends on temperature:

$$T_{06} = \frac{\dot{m}_{core}\, c_{p,c}(T_{05,core}, T_{06})\, T_{05,core} + \dot{m}_{duct}\, c_{p,d}(T_{0,duct}, T_{06})\, T_{0,duct}}{\dot{m}_{core}\, c_{p,c} + \dot{m}_{duct}\, c_{p,d}} \tag{39}$$

The mixer exit stagnation pressure is:

$$P_{06} = \pi_{mix}\, P_{05,core} \tag{40}$$

where π_{mix} is the mixer pressure ratio. The mixed exit mass flow is:

$$\dot{m}_{06} = \dot{m}_{core} + SR \cdot \dot{m}_{bypass} \tag{41}$$

2.7 Afterburner

The afterburner is modeled using the same combustor class as the main combustion chamber, with an independently specified reheat temperature $T_{07,AB}$ and afterburner efficiency η_{AB}. The afterburner pressure ratio π_{AB} accounts for the total pressure loss due to flame-holding hardware and heat addition. The additional fuel mass flow is computed from Eq. (30) applied to the mixed exit stream. When the afterburner is inactive, the class passes all thermodynamic quantities unchanged to the downstream nozzle.

2.8 Nozzle

IGNIT3 implements two nozzle types — variable-area (convergent–divergent) and fixed-area (convergent) — through a single class governed by a type flag. For the variable-area nozzle, the exit pressure is set equal to the ambient pressure, ensuring perfectly expanded flow:

$$P_{exit} = P_{\infty} \tag{42}$$

The exit temperature is found by solving the isentropic expansion with nozzle efficiency η_n:

$$\frac{T_{exit}}{T_{0,inlet}} = \left(\frac{P_{\infty}}{P_{0,inlet}}\right)^{(\gamma-1)/\gamma} \tag{43}$$

For the fixed-area convergent nozzle, the throat conditions are first evaluated assuming choked flow:

$$T_{throat} = \frac{2\,T_{0,inlet}}{1+\gamma} \tag{44}$$

The choking pressure is:

$$P_{choke} = P_{0,inlet}\left(1+\frac{1-\gamma}{\eta_n(1+\gamma)}\right)^{\gamma/(\gamma-1)} \tag{45}$$

If $P_{choke} > P_\infty$ the nozzle is choked and $P_{exit} = P_{choke}$; otherwise the nozzle is unchoked and the exit area is solved iteratively to find the off-design operating point.

3. Results

To assess the capabilities of the proposed thermodynamic cycle analysis framework, two representative propulsion systems were analyzed: a low-bypass turbofan engine representative of modern fighter aircraft applications and a high-bypass turbofan representative of commercial transport aircraft. The objective of these case studies is not to perform a direct performance comparison between the two engines, since they are designed to satisfy fundamentally different mission requirements, but rather to evaluate whether the framework reproduces the expected thermodynamic behavior associated with each propulsion architecture.

3.1 Demonstration cases

The fighter engine was configured with a low-bypass ratio turbofan and an afterburner located downstream of the turbine. Such engines are designed to maximize specific thrust and provide rapid acceleration, particularly during combat maneuvers and supersonic flight conditions. The addition of the afterburner allows supplementary fuel to be injected into the exhaust stream, significantly increasing the exhaust gas temperature and jet velocity. Although this process results in a substantial increase in thrust, it also leads to higher fuel consumption and lower overall efficiency. Consequently, military engines prioritize performance and thrust generation over fuel economy.

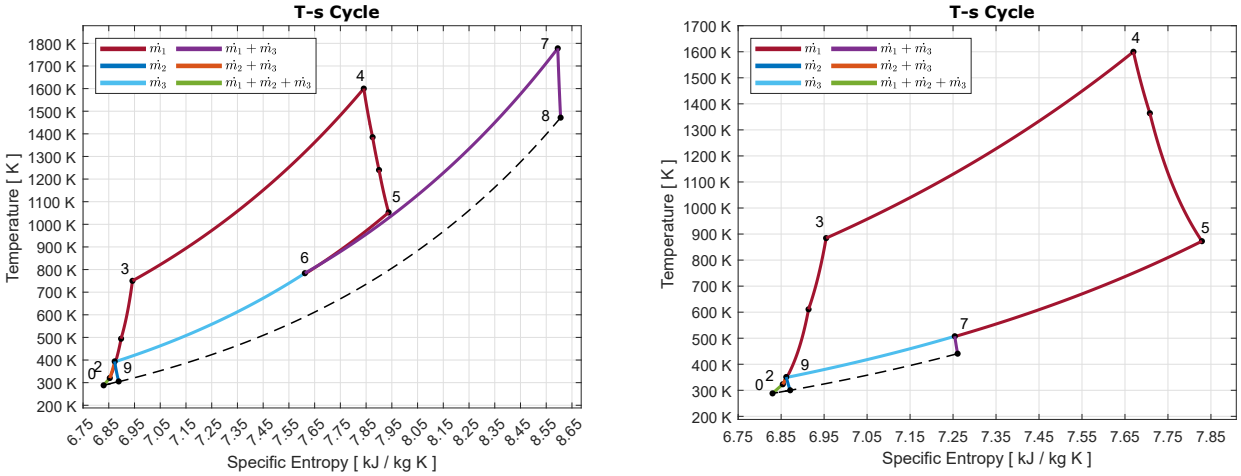
In contrast, the commercial turbofan was modeled as a high-bypass engine. Modern transport aircraft engines are optimized to maximize propulsive efficiency and minimize fuel consumption during long-duration cruise operations. The large bypass ratio enables a significant fraction of the total thrust to be generated by the fan stream, allowing the engine to produce the required thrust with a lower exhaust jet velocity. This design philosophy results in lower specific thrust but substantially improved fuel efficiency when compared with military propulsion systems.

Table 2 summarizes the main input parameters adopted for both engine configurations at design point (take-off). It should be noted that both engine configurations were analyzed using the same turbine inlet temperature (TIT). This assumption was intentionally adopted to facilitate a clearer comparison of the influence of engine architecture on overall cycle behavior. By maintaining the same maximum core temperature, the observed differences in performance can be primarily attributed to factors such as bypass ratio, flow mixing, nozzle expansion characteristics, and the presence of an afterburner, rather than variations in combustor exit temperature.

Note that the fighter engine exhibits larger jet velocities, and greater specific thrust as a direct consequence of its low bypass ratio and afterburning operation. The commercial engine, on the other hand, achieves superior propulsive efficiency and lower thrust-specific fuel consumption through the use of a large bypass stream and lower exhaust velocity. These trends accurately reflect the performance characteristics observed in real-world military and civil turbofan engines. Although the absolute values cannot be directly compared due to the different mission requirements of the two engines, the resulting trends are fully consistent with established gas turbine theory [1, 12].

Table 2 – Engine characteristics at design point (take-off).

Configuration	**Fighter Turbofan**	**Commercial Turbofan**
Mass Flow Rate $[kg/s]$	74.8	165
Bypass Ratio	0.75	10
Overall Pressure Ratio	25:1	40:1
Fan Pressure Ratio	3.5	1.6
Turbine Inlet Temperature $[K]$	1600	1600
Afterburner	On	Off
Net Thrust $[N]$	105352	126460
Specific Thrust $[N-s/kg]$	1423.68	766.43
Jet velocity (core) $[m/s]$	975.5	352.7
Jet velocity (fan) $[m/s]$	474.2	310.9
TSFC	0.153	0.0523
Propulsive Efficiency	0.0739	0.472
Thermal Efficiency	0.0192	0.301



(a) Fighter Turbofan.

(b) Commercial Turbofan.

Figure 2 – Temperature–entropy (T-s) diagrams.

3.2 On-design condition

Figure 2 presents the temperature–entropy (T-s) diagrams generated by the proposed framework for the two demonstration cases considered in this work: a low-bypass afterburning military turbofan (left) and a high-bypass commercial turbofan (right). The diagrams provide a graphical representation of the thermodynamic evolution of the working fluid throughout the engine and illustrate the ability of the framework to model different propulsion architectures within a unified simulation environment.

For both engines, the cycle begins with the intake and compression processes, represented by the nearly vertical segments between stations 2 and 3. The increase in temperature and pressure associated with the fan and compressor stages results in a moderate entropy rise due to component inefficiencies. The subsequent combustion process, extending from station 3 to station 4, produces the largest temperature increase in the cycle as fuel is added to the compressed air stream at approximately constant pressure.

Following combustion, the expansion through the turbine stages extracts energy from the gas stream to drive the compressor and fan. This process is characterized by a reduction in temperature accompanied by a gradual increase in entropy resulting from turbine irreversibilities. The most notable feature of the military engine cycle is the presence of the afterburner. After the core flow exits the tur-

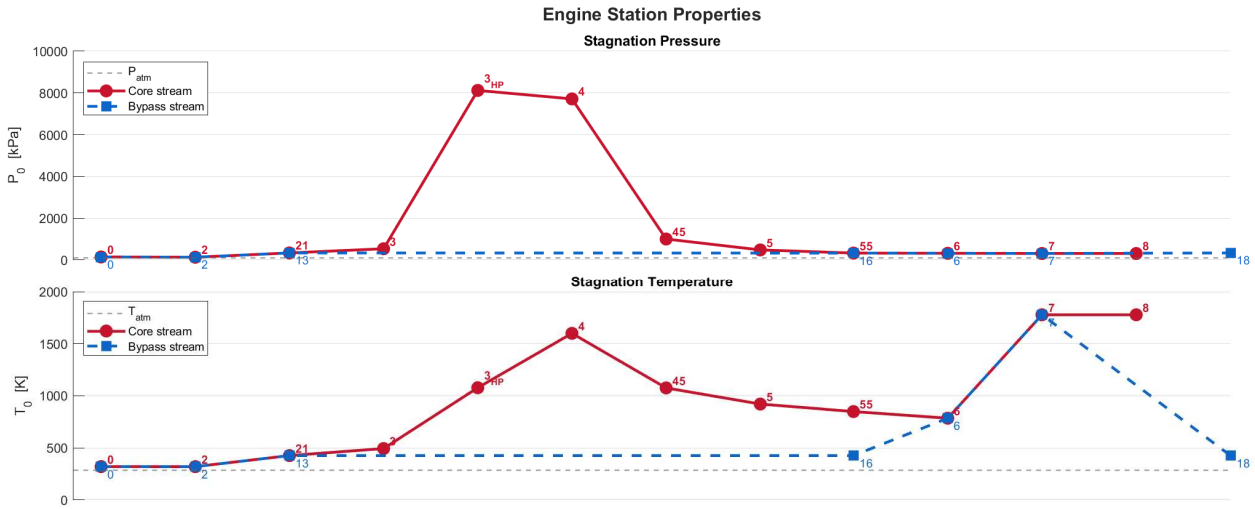


Figure 3 – Evolution of stagnation pressure and stagnation temperature along the engine stations for fighter turbofan.

bine, additional fuel is injected downstream of the turbine section, producing a second heat-addition process between stations 6 and 7. This process substantially increases the exhaust gas temperature before nozzle expansion, resulting in a significantly larger available energy drop across the nozzle. The subsequent expansion process from station 8 to station 9 generates a high exhaust jet velocity, which is characteristic of military propulsion systems designed for maximum specific thrust and high-performance flight conditions.

The commercial turbofan cycle exhibits a different behavior. Owing to the high bypass ratio, a significant portion of the airflow bypasses the combustor and turbine and follows a separate fan stream. The bypass flow is represented by the light-blue curve, while the core flow follows the conventional gas-generator cycle. The two streams are mixed downstream, as indicated by the transition between stations 7 and 9. Unlike the military engine, no afterburning process is present, and the exhaust gases enter the nozzle at considerably lower temperatures. Consequently, the commercial engine relies primarily on accelerating a larger mass flow rate rather than producing extremely high jet velocities, leading to superior propulsive efficiency and reduced fuel consumption.

A comparison of the two diagrams clearly highlights the distinct design philosophies of military and commercial propulsion systems. The military engine achieves high specific thrust through elevated exhaust temperatures and afterburning, whereas the commercial engine prioritizes fuel efficiency through a large bypass stream and lower exhaust velocities. The thermodynamic behavior predicted by the framework is consistent with the expected characteristics of modern turbofan engines, demonstrating that the integrated model reproduces the expected thermodynamic processes and interactions governing modern turbofan engine operation.

Figures 3 and 4 present the evolution of stagnation pressure and stagnation temperature throughout the engine stations for the military and commercial turbofan configurations, respectively. The plots separately track the thermodynamic states of the core and bypass streams, providing a detailed representation of the energy transfer processes occurring within each propulsion system.

For both engines, the stagnation pressure increases progressively through the fan and compressor stages, reaching its maximum value at the compressor exit. The subsequent pressure losses across the combustor are visible as a modest reduction in stagnation pressure before the turbine section. As expected, the turbine stages produce the largest pressure drop in the core stream, reflecting the extraction of energy required to drive the compressor and fan. The bypass stream, in contrast, experiences only a moderate pressure rise through the fan and remains largely unaffected by the

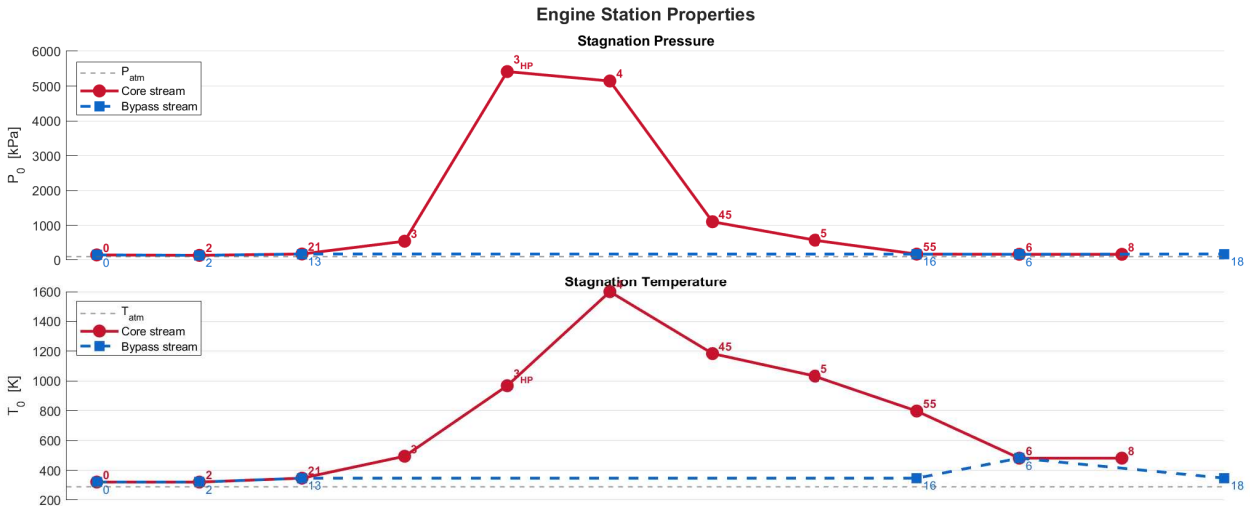


Figure 4 – Evolution of stagnation pressure and stagnation temperature along the engine stations for commercial turbofan.

core engine processes.

The stagnation temperature distributions exhibit the characteristic behavior of turbofan engines. The compression process increases the stagnation temperature of the core flow, while the combustor introduces a substantial temperature rise, bringing the flow to the prescribed turbine inlet temperature. Downstream of the combustor, the turbine stages progressively reduce the stagnation temperature as work is extracted from the gas stream.

The military engine, shown in Fig. 3, exhibits an additional temperature increase downstream of the turbine section due to the activation of the afterburner. This secondary heat-addition process raises the exhaust temperature significantly above the turbine exit value, providing additional energy for nozzle expansion and resulting in increased specific thrust. The associated pressure losses across the afterburner are also visible in the stagnation pressure distribution. This behavior is consistent with the operation of modern military propulsion systems, where afterburners are employed to temporarily augment thrust during high-performance flight conditions.

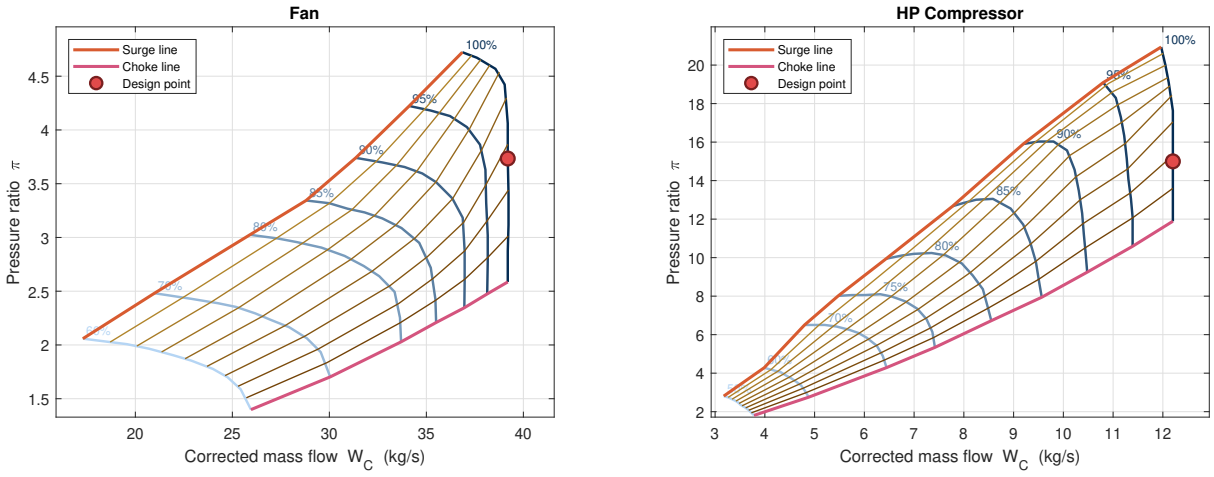
A comparison of the two figures highlights the fundamentally different propulsion strategies adopted by the two engine classes. Although both engines operate with the same turbine inlet temperature, the military configuration achieves higher exhaust temperatures through afterburning, whereas the commercial engine relies on a large bypass stream to maximize propulsive efficiency.

3.3 Off-Design performance

Figures 5 X and 6 present the fan and high-pressure compressor operating maps used in the off-design analysis of the military and commercial turbofan engines, respectively. The design-point operating conditions are indicated by the red markers, while the surge and choke lines define the boundaries of the stable operating region. The intermediate curves correspond to corrected rotational speed lines.

For both engine configurations, the design-point operating conditions lie within the stable region of the maps and maintain adequate margins from both the surge and choke boundaries. This behavior indicates that the selected cycle parameters are consistent with realistic compressor and fan operation and provides confidence in the off-design matching procedure implemented in the framework.

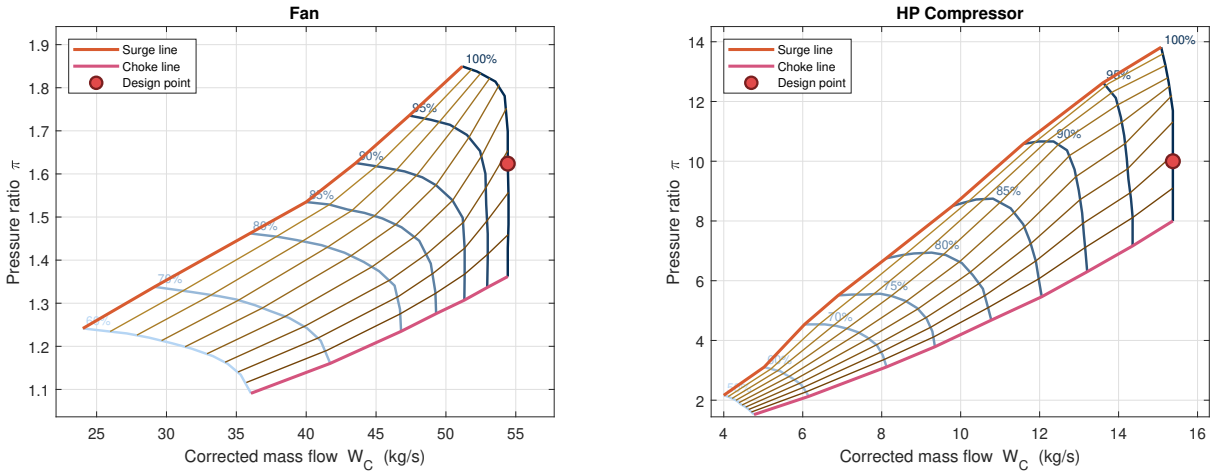
The fighter turbofan operates at high fan and compressor pressure ratios, reflecting the design objective of maximizing specific thrust. The fan design point is located near a pressure ratio of approxi-



(a) Fan map.

(b) HPC map.

Figure 5 – Off-design maps for fighter turbofan.



(a) Fan map.

(b) HPC map.

Figure 6 – Off-design maps for commercial turbofan

mately 3.6, while the high-pressure compressor achieves a pressure ratio close to 15. These values are representative of low-bypass military propulsion systems, where a greater proportion of the thrust is generated by the core stream and high compressor pressure ratios are desirable to improve cycle performance.

In contrast, the commercial turbofan exhibits a substantially lower fan pressure ratio, approximately 1.6, combined with a significantly larger corrected mass flow rate. This behavior is characteristic of high-bypass engines, which generate thrust by accelerating a large mass of air through the fan rather than by producing extremely high exhaust jet velocities. The high-pressure compressor also operates at a lower pressure ratio than that of the military engine, consistent with the reduced specific thrust requirements of commercial transport aircraft.

A comparison of the two sets of maps clearly illustrates the different propulsion strategies adopted by military and commercial turbofan engines. The military engine favors higher pressure ratios and greater energy addition within the core stream, whereas the commercial engine emphasizes large mass flow rates and efficient thrust generation through the bypass stream. The resulting operating

points are physically consistent with the intended applications of both engine architectures and further demonstrate the capability of the proposed framework to perform off-design performance analyses using component performance maps.

4. Conclusions

This paper presented IGNIT3, a modular thermodynamic framework for the performance analysis of aircraft gas turbine engines. The framework was developed using an object-oriented architecture in MATLAB, allowing individual engine components to be modeled as independent modules that can be assembled into a wide range of propulsion system configurations. The implemented methodology includes the simulation of intake systems, fans, compressors, combustors, turbines, mixers, afterburners, and nozzles, together with the capability to evaluate both design-point and off-design operating conditions.

The capabilities of the framework were demonstrated through two representative case studies: a low-bypass afterburning military turbofan and a high-bypass commercial turbofan. The resulting performance predictions, temperature–entropy diagrams, station property distributions, and component operating maps exhibited trends that are consistent with established gas turbine theory. In particular, the analyses successfully captured the distinct thermodynamic characteristics associated with each propulsion architecture, including the effects of bypass ratio, flow mixing, turbine work extraction, nozzle expansion, and afterburning.

The off-design analyses further demonstrated the ability of the framework to integrate component performance maps and evaluate operating conditions within realistic compressor and fan operating envelopes. The predicted operating points remained within stable regions of the corresponding maps, illustrating the suitability of the implemented matching procedures for engine performance assessment beyond the design point.

A key advantage of the proposed framework is its modular structure, which facilitates the rapid evaluation of alternative propulsion architectures and technology concepts. The implementation allows new components and thermodynamic models to be incorporated with minimal modifications to the overall code structure, making the framework suitable for both educational and research applications.

Beyond conventional turbofan engines, the framework provides a foundation for the investigation of emerging propulsion technologies and future sustainable aviation concepts. Potential applications include the assessment of alternative fuels, such as sustainable aviation fuels (SAFs) and hydrogen, as well as the analysis of advanced propulsion architectures incorporating intercooling, recuperation, variable-cycle engines, hybrid-electric systems, distributed propulsion, and boundary-layer ingestion concepts.

Furthermore, the computational efficiency and modularity of the framework make it particularly attractive for integration with multidisciplinary design optimization environments. The ability to rapidly evaluate engine performance across a broad design space enables its use in propulsion system sizing, cycle optimization, aircraft-engine integration studies, and technology trade-off assessments during the conceptual and preliminary design phases.

Future developments will focus on the incorporation of higher-fidelity component models, expanded fuel-property databases, additional off-design capabilities, and coupling with optimization algorithms to support the design and assessment of next-generation aircraft propulsion systems.

5. Contact Author Email Address

mailto: pdbravom@usp.br

6. Copyright Statement

The authors confirm that they, and/or their company or organization, hold copyright on all of the original material included in this paper. The authors also confirm that they have obtained permission, from the copyright holder of any third party material included in this paper, to publish it as part of their paper. The authors confirm that they give permission, or have obtained permission from the copyright holder of this paper, for the publication and distribution of this paper as part of the ICAS proceedings or as individual off-prints from the proceedings.

References

[1] Jack D Mattingly. *Aircraft engine design*. AIAA, 2002.

[2] Mark Guynn, Jeffery Berton, Kenneth Fisher, William Haller, Michael Tong, and Douglas Thurman. Analysis of turbofan design options for an advanced single-aisle transport aircraft. In *9th AIAA Aviation Technology, Integration, and Operations Conference (ATIO) and Aircraft Noise and Emissions Reduction Symposium (ANERS)*, page 6942, 2009.

[3] Jeffryes W Chapman, Thomas M Lavelle, and Jonathan S Litt. Practical techniques for modeling gas turbine engine performance. In *52nd AIAA/SAE/ASEE joint propulsion conference*, page 4527, 2016.

[4] Tomas Grönstedt. *Development of methods for analysis and optimization of complex jet engine systems*. Chalmers Tekniska Hogskola (Sweden), 2000.

[5] KH Liew, E Urip, and SL Yang. Parametric cycle analysis of a turbofan engine with an interstage turbine burner. *Journal of propulsion and power*, 21(3):546–551, 2005.

[6] Scott M Jones. An introduction to thermodynamic performance analysis of aircraft gas turbine engine cycles using the numerical propulsion system simulation code. Technical report, NASA, 2007.

[7] Scott M Jones. Steady-state modeling of gas turbine engines using the numerical propulsion system simulation code. In *Turbo Expo: Power for Land, Sea, and Air*, volume 43963, pages 89–116, 2010.

[8] Scott M Jones. Development of an object-oriented turbomachinery analysis code within the npss framework. Technical report, NASA, 2014.

[9] Hatim Soeb Rangwala and Donald Wilson. Simulation of a low-bypass turbofan engine with an ejector nozzle using npss. In *53rd AIAA/SAE/ASEE Joint Propulsion Conference*, page 5056, 2017.

[10] Eric S Hendricks and Justin S Gray. pycycle: A tool for efficient optimization of gas turbine engine cycles. *Aerospace*, 6(8):87, 2019.

[11] Tristan A Hearn, Eric Hendricks, Jeffrey Chin, and Justin S Gray. Optimization of turbine engine cycle analysis with analytic derivatives. In *17th AIAA/ISSMO Multidisciplinary Analysis and Optimization Conference*, page 4297, 2016.

[12] Ronald D Flack. *Fundamentals of jet propulsion with applications*, volume 17. Cambridge University Press, 2005.

[13] Robert M Plencner. Plotting component maps in the navy/nasa engine program (nnep): A method and its usage. Technical report, 1989.

[14] Mohammad Razmjooei, Fathollah Ommi, et al. Experimental analysis and modeling of gas turbine engine performance: Design point and off-design insights through system of equations solutions. *Results in Engineering*, 23:102495, 2024.